Rapid synthesis of polymer-silica hybrid nanofibers by biomimetic mineralization

Pritesh A. Patel [a], Jessica Eckart [b], Maria C. Advincula [c], A. Jon Goldberg [c], Patrick T. Mather [a,d,*]

[a] Department of Macromolecular Science and Engineering, Case Western Reserve University, United States
[b] Department of Biomedical Engineering, Case Western Reserve University, United States
[c] Center for Biomaterials, Department of Reconstructive Sciences, University of Connecticut Health Center, United States
[d] Syracuse Biomaterials Institute and Biomedical and Chemical Engineering Department, Syracuse University, Syracuse, NY 13244, United States

ARTICLE INFO

ABSTRACT

Biomimetic formation of silica from polyamines such as poly(ethylene imine) (PEI), inspired by the proteins found in diatoms and sponges, has been actively investigated recently as a potential route to silica formation compared to the conventional sol–gel process. We report silica formation onto nanofibers of PEI blended with poly(vinyl pyrrolidone) (PVP) obtained via electrospinning of their 50:50(w/w) blend. The active component, PEI, catalyzes rapid silica formation, within minutes, upon immersion of the PEI/PVP nanofibers in silica precursor tetramethylorthosilicate (TMOS). The silica formation in nanofibers was then investigated by scanning electron microscopy (SEM), Energy Dispersive X-ray analysis (EDX), differential scanning calorimetry (DSC), thermo-gravimetric analysis (TGA) and Fourier-transform infra-red (FTIR) spectroscopy. The silica content in the PEI/PVP nanofibers could be controlled by pre-treatment of the fibers at different conditions of relative humidity prior to the silicification. Fibers exposed at higher (80%) relative humidity led to higher inorganic (silica) content compared to those exposed to relative dry conditions (<20% relative humidity). Calcination of the fibers indicated that silicification proceeded across the whole fiber cross-section that consisted of nano-structured silica. Such a simple route to rapid formation of organic-inorganic hybrid nanofibers could have applications ranging from catalysis to tissue engineering, and nanocomposites in general.

© 2009 Elsevier Ltd. All rights reserved.

1. Introduction

Nature excels in the design and synthesis of complex and hierarchical hybrid (organic/inorganic) materials for various functional purposes through biomineralization processes [1–3]. Such hybrid materials like bone, mollusk seashell, nacre, and silica structures in diatoms and sponges have inspired researchers to mimic their structure and function for various applications [4–6]. In such hybrid materials, organic molecules are closely integrated with inorganic moieties for various structural and functional purposes [7,8]. In particular, the formation of natural hybrid materials is often regulated by proteins that catalyze inorganic formation while spatially directing or templating the growth of hierarchical structures. Proteins, for example, like silaffins found in various species of diatoms, regulate silica growth to form species-specific nano-structured composite materials [9,10]. Such functional protein serves two purposes: (i) catalyze silica polymerization, and (ii) act as templating agents by self-assembly to direct the growth of silica [9,11]. Both of these functional aspects have been extensively studied by various researchers to design biomimetic materials for various applications.

Nano-structured silica composites represent one such class of hybrid organic/inorganic material with various applications that include catalysis [12], sensors [13], photonics [14], biomaterials [15], biotechnology and medicine [16], among many other applications [17]. Conventionally, most such hybrid materials are synthesized by a sol–gel process [18,19]. By this method, hydrolyzed sol–gel precursors are condensed onto templates formed by organic molecules (a process termed transcription) that include spherical polymer particles or crystals [20], tri-block copolymers [21], and organo-gelators [22] to form structured composites (for an informative review see [23]). The templating route utilizes specific interactions like hydrogen bonding and/or electrostatic interactions between the hydrolyzing sol–gel precursor and the templating substrate to integrate the organic and inorganic components. Besides such template transcription, electro-processing (or electrospinning) offers

the potential to produce ceramic and hybrid nanocomposites [24–26]. In this method, aged (partially reacted) sol–gel precursor solutions or their blends with polymers like poly(vinyl pyrrolidone) (PVP) are electrospun to produce ceramic or composite nanofibers, respectively. Various studies have shown that such sol–gel electro-processing can form inorganic and ceramic nanotubes or nanofibers of alumina/silica [27], titania [28], and bioactive glass [15]. Despite the advantages with sol–gel processing to obtain composite and ceramic nanofibers, it requires relatively harsh conditions of temperature and/or pH with acid/base catalysts and is an inherently time-consuming process. For example, silica vesicles made by electrospinning (e-spinning) of aged sol in a study by Larsen et al. [27] required a total of 14 h including 2 h at 80 °C to prepare aged sol in HCl-catalyzed reaction of tetraethylorthosilicate (TEOS). On the other hand, biomimetic processes are usually executed with benign conditions of near-neutral or slightly acidic pH and are rapid, thus offering advantages to the design and synthesis of silica-based materials.

Recent findings provide insight to simpler alternative biomimetic routes for silica formation, creating the potential for development of nano-structured composite materials at biocompatible conditions and higher rates. Proteins isolated from marine species such as diatoms and sponges were found to facilitate (or catalyze) the formation of silica from hydrolyzed precursor tetraalkoxysilanes [29,30]. The functional units responsible for the rapid silica precipitation have been identified as polylysine residues covalently modified by the oligo-N-methyl-propylamine unit [9]. These modifications play a central role in the silica precipitating activity of the native enzyme. Catalytic domains in the protein, primarily consisting of polyamines, self-assemble in specific spatial arrangements and direct silica growth in the diatoms. In one such proposed mechanisms, the polyamines catalyze the silica formation due to the alternating presence of protonated and non-protonated amine groups in the polyamine chains, which allows hydrogen bond formation with the oxygen adjacent to silicon in the precursor and thus facilitate –Si–O–Si– bond formation [11]. The importance of polyamines in silica precipitation has led to the development of various bio-inspired molecules, synthetic proteins, polypeptides, block copolypeptides, and small functional molecules containing polyamines that catalyzes silica [31]. The time-scale of silica precipitation in the presence of such molecules varies depending on the type of functionality and silica precursor. The majority of biomimetic silica formation has been studied in the presence of a pre-hydrolyzed precursor, usually by acid/base catalysis rather than directly from pure alkoxysilanes. On other hand, poly(ethylene imine) (PEI), linear and branched, has the ability to form silica directly from pure alkoxysilanes such as tetramethylorthosilicate (TMOS) almost instantly in aqueous solutions [32,33]. Additionally, linear PEI can form fibrous aggregates because of its propensity to crystallize in aqueous media above a concentration of 0.5 wt% [34]. Such aqueous linear PEI aggregates have also been shown to induce a hydrolytic condensation of TMOS and create silica of different morphologies depending on the concentration of alkoxysilanes, water, and solvent [33,35]. It was also shown that the silica formed on the crystalline PEI filaments have a 5–7 nm core containing PEI fibrils with a 6–8 nm thick silica shell [36].

Based on the above results, we hypothesized that silicification on electrospun fibers of PEI or its blends would lead to a process that induces rapid silica formation to form hybrid (polymer/silica) materials. Such process would combine the benefits of electro-processing techniques with rapid silica formation directly from precursor molecules, as observed previously in solutions, to obtain hybrid materials. Compared to the processes described above in literature, the hybrid nanofibers formation is rapid, and without

requiring use of high temperature and/or extreme pH in solutions. Herein, we report the formation of hybrid (organic/inorganic) materials obtained from direct silicification of linear PEI/PVP fibers obtained by electro-processing of their 50/50 (w/w) blend. PVP was used as a carrier blend component to assist in the formation of stable nanofibers at ambient operating conditions that resisted flash welding and subsequent film formation. Unlike the PEI/PVP nanofibers, nanofibers of PEI alone were unstable to film formation at ambient conditions due to excessive moisture adsorption. The selection of PVP as a blend component was further dictated by its miscibility with PEI and its solubility in ethanol solutions utilized in the electro-processing. The silicification of PEI/PVP fibers was done by immersing the fibers in TMOS. TGA, EDX and FTIR analysis confirmed the presence of the silica. The control sample of PVP fibers did not form any silica, confirming that PEI catalyzes the silica polymerization reaction. Furthermore, the silica content in the PEI/PVP nanofibers could be controlled by pre-treatment of the fibers at different humidity levels prior to the silicification. Calcination of the fibers revealed that silicification proceeded across the whole fiber cross-section rather than just the surface (outer shell) of the fibers.

2. Experimental section

2.1. Synthesis of linear poly(ethylene imine)

Linear PEI was synthesized from the precursor poly(2-ethyl-2-oxazoline) (PeOz) (Polysciences, $Mw = 500$ kDa) according to a previously reported procedure [33]. In brief, PeOz was hydrolyzed in a 5 M HCl solution with a 3:1 molar ratio of HCl to acetylethyleneimine units at 90 °C for 12 h (polymer concentration = 0.145 g/ml). A white precipitate formed during the reaction and was filtered and washed with acetone, followed by dissolution in ultra-pure deionized (DI) water (Milli-Q, $\rho > 18$ MΩ cm^{-1}). The solution was either directly neutralized with the addition of 0.5 M KOH or sealed in a dialysis tube (Spectroline, Mw cut-off 3500 Da) and dialyzed against a 14% aqueous ammonia solution for 3 days, replacing the solution every 24 h. In both cases, the white precipitate obtained was filtered, washed with excess acetone and DI water, and dried in vacuum at 40 °C for 24 h. The conversion of oxazoline (Oz) in PeOz to imine in PEI was characterized by ^{1}H NMR spectroscopy (Varian Inova 600 MHz) in CD$_3$OD at room temperature by evaluating the Oz peaks ($\delta_H = 2.4$ ppm, –CH$_2$– and $\delta_H = 1.1$ ppm, –CH$_3$) relative to the ethyleneimine peak ($\delta_H = 2.74$ ppm). Additionally, the ethyl protons adjacent to nitrogen in PeOz ($\delta_H = 3.5$ ppm, –CH$_2$CH$_2$N–Oz–) shift upon conversion to PEI ($\delta_H = 2.74$ ppm, –CH$_2$CH$_2$ND–). The conversion of the oxazoline units to ethyleneimine units was 94%, irrespective of the precipitation method used.

2.2. Electrospinning of PEI/PVP blend

Electrospinning (e-spinning) of linear PEI solutions in ethanol spanning 5–15 wt% in concentration resulted in sub-micron fibers (here termed "nanofibers") that quickly absorbed moisture at ambient conditions due to hygroscopic nature of the PEI. This eventually led to the formation of films by 'flash welding' of the fibers [see Supplementary information Figure S1]. In order to obtain fibers stable at ambient conditions, a second miscible polymer was incorporated. Linear PEI was solution-blended with poly(vinyl pyrrolidone) (PVP) (Mw 350,000 Da) (Aldrich). Nanofibers stable to even humid environments were obtained by e-spinning of linear PEI/PVP (50/50 w/w) blends in 5–15 wt% concentrated solutions in ethanol at a flow rate between 0.1 ml/h and 0.4 ml/h, a voltage gradient 0.8 kV cm^{-1} over the 10 cm distance between the tip and the collector, and processing time of

3 h. For e-spinning, polymer solutions of a given concentration were pumped through a stainless steel needle (I.D. 0.26 mm) using a syringe pump (KD Scientific, Model 780100) at a specified flow rate. The needle was held at high electric potential relative to ground using a high voltage power supply (0–20 kV, Ultravolt, Model 30A12-P4) and controlled by a DC power supply (0–6 V, Agilent, Model E3630A). The samples were collected in a steel (SS type 304) mesh (screen) of square shape with area ∼25 cm^2, wire gauge of 40 × 40 meshes per linear inch, and wire size 0.0075 inch (Custom Filtration Inc, MN) for approximately 3 h.

2.3. Silicification and calcination

Silicification of the resulting nanofibers was accomplished by immersing the fiber mats (on a supporting mesh) in tetramethyl orthosiliciate (TMOS) for 10 min, unless specified otherwise, followed by rinsing with excess acetone multiple times followed by drying in vacuum at 40 °C for at least 4 h. The silica content of the PEI/PVP fibers after equilibration at various relative humidity values was studied by exposing the fiber mats to different controlled humidity conditions for at least 24 h prior to silicification and then immersing the fiber mats into the TMOS for silicification. Controlled humidity conditions were achieved by use of a small chamber within which aqueous lithium chloride solutions (0.143 g LiCl/ml for 80% relative humidity and 0.367 g LiCl/ml for 40% relative humidity) or desiccant (for relative humidity <20%) were placed. For the chamber with desiccant, the relative humidity fluctuated between 10% and 20% and hence is reported to be <20% in the text. The humidity was measured by digital hygrometer (Traceable® Control Company, TX). The silicified fibers were removed from the mesh after drying for subsequent calcinations and other characterization. Calcination of the silicified nanofibers was then achieved by heating the fiber mats in a crucible to the 600 °C in a furnace for 1 h. The resulting materials were fragile and required careful handling.

2.4. SEM–EDX

The electrospun nanofibers were analyzed using a Scanning Electron Microscopy (SEM) (Philips XL30 Environmental SEM) before and after silicification. The average and standard deviation (SD) of fiber diameter from SEM images were calculated using ImageTool™ (v3.0) image processing software for total of 50 diameter measurements. Pixel dimensions of the images were calibrated from the scale bar in the image. Calcined fibers were imaged using high resolution SEM (Field-Emission Gun Scanning Electron Microscope Hitachi S4500). For both cases of SEM measurements, prior to analysis, samples were sputter coated with palladium for 30 s using a current of 45 mA under argon at a pressure of approximately 200 mTorr, yielding a coating thickness ca. 50 Å. Elemental analysis was performed using Energy Dispersive X-ray (EDX) probe attached to the same SEM described above.

2.5. Thermal characterization

The nanofiber webs were characterized using a TA Instruments Q500 thermo-gravimetric analyzer (TGA) heating at rate of 20 °C/min from room temperature to 1000 °C. The inorganic (silica) fraction of the silicified samples was measured by calculating the weight percentage remaining at 900 °C in the TGA thermograms. Fourier-transform infra-red analysis (FTIR) was performed by a potassium bromide (KBr) pellet method. KBr pellets were made by mixing ∼1 mg of sample with 90 mg of FTIR-grade KBr. FTIR (Thermo Nicolet – Nexus 870) spectra of the prepared KBr pellets were recorded with a range of wave numbers spanning 400 cm^{-1}–4000 cm^{-1} with averaging over 64 scans.

Thermal analysis of LPEI, PVP, e-spun LPEI/PVP nanofibers and silicified LPEI/PVP nanofibers to determine melting temperatures (T_m) and latent heats of fusion (ΔH) was performed using differential scanning calorimetry (DSC, TA Instruments Q100 equipped with a refrigerated cooling accessory) under a nitrogen purge. The samples were cooled quickly to −50 °C, heated from −50 °C at rate of 10 °C/min to 180 °C (first heat or "1H"), followed by subsequent cooling to −50 °C at the same rate (first cool or "1C"). Next, these steps were repeated to obtain DSC thermograms for a second cycle at same rate. The PEI and the silicified PEI/PVP nanofibers underwent the same heating/cooling profile but with restriction to a temperature maximum of 100 °C due to weight loss of the samples (>0.5 wt%) occurring above that temperature. All DSC data analyses were performed using TA Instruments Universal Analysis software (v4.5).

3. Results

Electrospun nanofibers of linear poly(ethylene imine) (PEI) and poly(vinyl pyrrolidone) (PVP) blends from their ethanol solutions were obtained using conditions specified above. Fig. 1(a–c) shows the SEM image of nanofibers obtained by e-spinning a PEI/PVP (50/50 w/w) solution in ethanol at a flow rate of 0.1 ml/h and at concentrations of 5 wt% and 10 wt%, respectively. Analysis of Fig. 1a obtained from the 5 wt% PEI/PVP solution indicates a broad diameter distribution, with an average diameter of 452 nm and standard deviation, SD, of 210 nm. Close inspection of the micrographs reveals that the large standard deviation values are a reflection of a bimodal diameter distribution, with the presence of relatively smaller diameter fibers along with larger fibers (Fig. 1a). The origin of such a bimodal distribution in the PEI/PVP fibers is not known. Increasing the concentration of the PEI/PVP solution to 10 wt% (Fig. 1b), while keeping other parameters constant, resulted in a narrower distribution of fiber diameters and a decrease in the average diameter to 285 nm (SD = 56 nm), compared to the 5 wt% solution. Such nanofibers are continuous and uniform in diameter over the entire length scale as evident from Fig. 1c. Thus, changing the concentration of the e-spinning solution allowed for control over the fiber diameter and the morphology of the resulting nanofibers. Besides concentration, e-spinning flow rate can also be used to manipulate fiber diameter and morphology [37]. For example, electrospinning fibers with a 10 wt% solution at a flow rate of 0.3 ml/h through an electric field of 0.8 kV cm^{-1} over a 10 cm tip-to-collector distance resulted in a large average diameter of 1147 nm (SD = 313 nm). Besides the increase in fiber diameter, increasing the concentration and/or flow rate for e-spinning solution also increases the web density of the fiber mats. The effect of web density on the silicification and subsequent hybrid fiber formation will be not considered in this paper, but does warrant future attention.

PEI/PVP nanofibers, shown in Fig. 1, were silicified by immersing in TMOS for 10 min, rinsing in excess acetone to remove unreacted TMOS, and finally drying at 40 °C for 4 h under vacuum. The PEI/PVP web became detectably stiffened by silicification. Fig. 2(a–c) shows the SEM images of silicified PEI/PVP fibers corresponding to the non-silicified samples of Fig. 1(a–c). Interestingly, our silicification process caused adjacent fibers to 'weld' at contact points [38], as evident in the SEM images shown in Fig. 2. It is assumed that such fiber welding due to silicification is different from the solvent flash welding, particularly evident in PEI only e-spun nanofibers (Supplementary Figure S1). Compared to 'flash-welded' silicified fibers, the non-silicified PEI/PVP fibers shown in Fig. 1(a–c) are intact and do not show flash welding. Additionally, the fiber diameters increased during silicification, with fibers obtained from
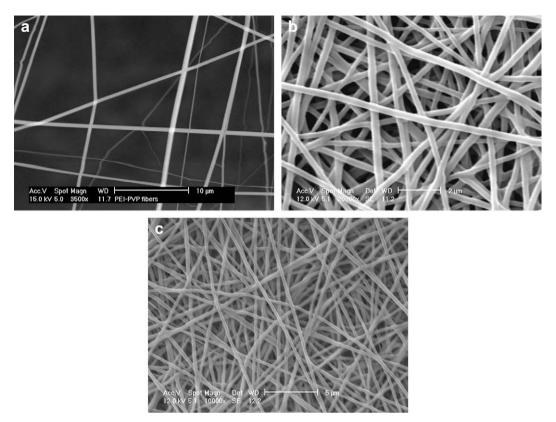
Fig. 1. SEM images of the fibers of the 50:50 blends of linear PEI and PVP in ethanol electrospun at concentration of (a) 5 wt% and (b, c) 10 wt%.
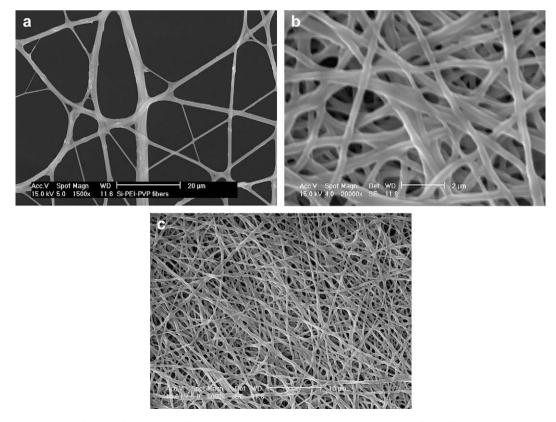

Fig. 2. SEM images of the silicified electrospun fibers of PEI:PVP (50:50) corresponding to the electrospun fibers of (a) Fig. 1a and (b, c) Fig. 1b.

the 5 wt% PEI/PVP solutions (Fig. 2a), showing a greater increase in diameter than fibers spun from the 10 wt% solution (Fig. 2b, c). For example, the fiber diameters in Fig. 2a, while having a similar distribution to those in Fig. 1a, almost tripled to 1383 nm (SD = 394 nm). In contrast, the average fiber diameter in Fig. 2b increased by ca. 100 nm to the value of 390 nm (SD = 96 nm) (see Supplementary information, Figure S2 for comparison of distribution). The observed difference may be due to the higher web density for the sample prepared from a 10 wt% solution as impingement may limit growth. Moreover, the equilibrium water content affects the level of silicification from PEI, as was verified by TGA analysis shown later, and it is possible (though unlikely) that the webs of Fig. 2 had different water contents prior to silicification. Nevertheless, rapid silica formation – within minutes – in the nanofibers was achieved by immersion of the fibers in pure TMOS.

PEI appears to have catalyzed the hydrolysis and condensation of TMOS to form silica during the short exposure of TMOS to electrospun PEI nanofibers for 10 min. To confirm this, EDX spectra of the fibers before and after silicification were collected and compared to a control sample of PVP fibers immersed in TMOS. The PVP fibers were obtained by electrospinning a 10 wt% PVP solution in ethanol using the same conditions described above for PEI/PVP nanofiber processing. After immersion in TMOS, such PVP fibers did not show any presence of elemental silicon in EDX analysis as seen in Fig. 3 and also showed no change in diameter; unlike the silicified PEI/PVP fibers (Supplementary Information, Figure S3). In contrast, EDX spectra of silicified PEI/PVP fibers showed a strong peak of elemental silicon present in the EDX spectra (Fig. 3). On other hand, the oxygen peak shows very little change upon silicification, but this is within experimental error. Specifically, elemental analysis showed that the atomic weight percent of silicon was ca. 58% and that of oxygen to be 42%, close to the values found for completely condensed silica (53.2% oxygen, 46.8% silicon). Nevertheless, the absence of silicon peak in the PVP fibers exposed to TMOS signifies further that the silicon peak seen in PEI/PVP
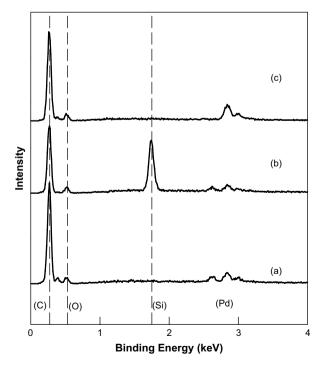
silicified fibers is not merely due to TMOS adsorption (that might have survived acetone wash) and/or silica formation by sol–gel hydrolysis and condensation without PEI catalyst. EDX results will be further supported by FTIR characterization, discussed below in reference to Fig. 7.

PEI – a crystalline polymer – retains substantial crystallinity in the electrospun nanofiber obtained from 50:50 blends with amorphous PVP. As evident from Fig. 4a and b (curve (i)), bulk PEI is crystalline with two distinct melting endotherms (T_{peak} = 47.3 °C and 65.8 °C) in the first cycle and a single melting endotherm (T_{peak} = 44.7 °C) in the subsequent second cycle. PVP, however, is an amorphous polymer as indicated by the absence of any melting endotherm in curve (ii) of Fig. 4a and b. Unlike PVP but similar to bulk PEI, an electrospun web of PEI/PVP nanofibers (Fig. 4a, curve (iii)) has multiple melting endotherms (T_{peak} = 60.6 °C and 80.5 °C). Consistent with the second DSC cycle of bulk PEI, a single melting endotherm is observed for the electrospun nanofibers (T_{peak} = 57.6 °C) (Fig. 4b, curve (iii)). We note that the broad endotherm in electrospun nanofibers at high temperature (ca. 100–110 °C) in the first cycle is likely due to evaporation of excess adsorbed water in the nanofibers. Such transition disappears in the subsequent second heat/cool cycles of the nanofiber (Fig. 4b). Nevertheless, Fig. 4b indicates that the presence of amorphous PVP in the PEI/PVP nanofibers does not hinder the formation of PEI crystals in the nanofibers. Furthermore, analysis of Fig. 4b indicates that the heat of fusion of PEI in nanofibers (ΔH = 55.4 J/g-PEI, curve (iii)) is substantially higher than bulk PEI (ΔH = 27.2 J/g, curve (i)). (Note: we have compared the latent heat of melting on a per-gram of PEI basis.)

Clearly, the electrospinning process, enhances the PEI crystallinity in the nanofibers compared to the bulk PEI. Interestingly, subsequent silicification of the nanofibers by TMOS exposure results in the disruption of the PEI crystals in the silicified nanofibers as indicated by small endotherm in Fig. 4b (curve (iv)). The heat of fusion of the silicified nanofiber is very low (ΔH = 4.1 J/g) compared to that of electrospun PEI/PVP nanofibers (ΔH = 55.4 J/g-PEI, curve (iii)). This analysis indicates that the crystalline PEI enhances or at least supports silica formation in the nanofibers. The observed results are consistent with various studies [32–36] of silica formation observed in linear PEI crystalline aggregates formed in aqueous solutions at low PEI concentrations (0.5–2 wt%). Our study reveals that the crystalline PEI has a similar ability to catalyze silica formation when present in nanofibers with amorphous PVP.

TGA experiments enabled further quantification of nanofiber silicification, as revealed in Fig. 5. It was found that the inorganic (silica) yield in the electrospun PEI/PVP nanofibers requires PEI and varies with water content in the fibers as evidenced by TGA analysis of fibers pre-treated with different levels of humidity before silicification (Fig. 5). We note that other sources of moisture may exist and were not directly controlled in our experiments, such as trace moisture in ethanol (during spinning) and TMOS, as well as moisture from the air following TMOS treatment but prior to vacuum drying. Consistent with EDX results discussed above, Fig. 5 reveals that the control PVP fibers after TMOS exposure had a negligible inorganic content of 4.7 wt% at 900 °C. Such inorganic formation could occur from the small amount of silica formation from residual TMOS at higher temperatures in TGA. Further, the non-silicified fibers did not show any inorganic content, as was expected. Depending on the pre-treatment of fibers at different relative humidity levels, the silica content was found to vary significantly. For example, fibers exposed to ca. 40% relative humidity prior to silicification yielded only 12 wt% inorganic (silica) content (at 900 °C) compared to 41 wt% for the fibers exposed to 80% relative humidity prior to silicification. Also, it was found that fibers exposed to 20% or less relative humidity before silicification yielded a negligible (2.6 wt%) presence of inorganic content.

Fig. 3. Energy Dispersive X-ray (EDX) spectra of (a) PEI/PVP (50/50 w/w) electrospun fibers, (b) after silicification by TMOS and (c) control sample of PVP fibers after TMOS exposure for 10 min. The vertical dotted line indicates the reference peak of the corresponding elements shown in bracket.
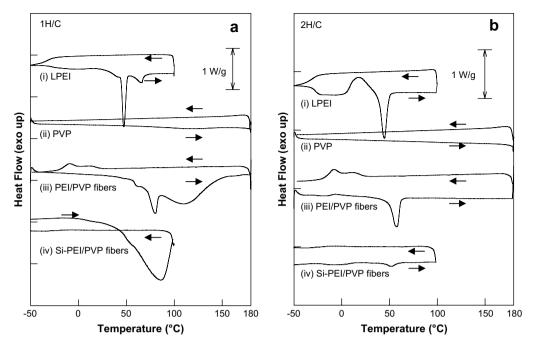
Fig. 4. DSC curve of the (a) first heating/cooling cycle and (b) second heating/cooling cycle of: (i) LPEI, (ii) PVP and (iii) LPEI/PVP e-spun fibers and (iv) Silicified LPEI/PVP e-spun fibers after TMOS immersion for 10 min. The heating and cooling is at rate of 10 °C/min.

We reason that the humidity level affects the equilibrium moisture content of the fibers, in turn affecting silicification via the hydrolysis of TMOS by PEI. As evident from Fig. 5 (curve (i)), a 18% weight loss of the PEI/PVP fibers occurs at temperatures below 120 °C, roughly indicating the level of water absorption by the fibers. Upon silicification (curves (iii) and (iv)), the weight loss at 120 °C decreases to 7–8 wt% due to the utilization of water in the hydrolysis. Note that PVP fibers are less hygroscopic than PEI and hence have a weight loss of only 4% at 120 °C. Water in the fibers gets consumed during hydrolysis and then later gets liberated during condensation of the silanol (Si–OH) groups to form siloxane (–Si–O–Si–) linkages due to PEI catalysis as well as self-condensation of silanol groups at higher temperatures. The latter phenomenon is evident from the significant weight loss observed (ca. 12 wt%) for the fibers exposed to 80% relative humidity (curve (iv)) between temperatures of 600 °C and 700 °C. While the TGA characterization allowed estimation of the water content of the fibers before and after silicification, as just discussed, the effect of water content and consumption on silica content of fibers warrants detailed attention, including time-dependent gravimetry. Nevertheless, the present study reveals that water in the fibers is important for rapid silicification by PEI and it indirectly provides a means to control the inorganic content of the fibers by direct mineralization.

Interestingly, silica formation in the nanofibers is not confined to the surface of such fibers but permeates the whole fiber cross-section, at least following calcination. Indeed, calcination of the silicified PEI/PVP nanofibers at 600 °C for 1 h led to the nano-structures within the fibers revealed by high resolution SEM (Fig. 6(a–d)). Here, we observe that the calcined fibers contained nanometer-sized silica fibrils across the whole fiber cross-section (Fig. 6a, b). Further, low magnification micrographs (Fig. 6c, d) revealed that the silicification/calcination of the fibers occurs uniformly over entire fiber cross-section and length. To our surprise, the fiber structure was mostly preserved, even though the fibers were fragile as evident from breaking of fibers seen in the low magnification images (Fig. 5c, d). The low mechanical integrity of the calcined fibers suggests that the nanostructures in the fibers are poorly interconnected. Nevertheless, calcination led to a uniformly

distributed porous nanostructure consisting of two length scales: the sub-micron fibers ($\sim$450 nm) and the silica nanostructures ($\sim$20 nm) with a relative ratio of silica 'fibrils' diameter to fiber diameter of about $D_{silica}/D_{fib} \sim 0.04$–$0.07$. Calcination of silica obtained from sol–gel condensation is known to result mostly in dense particles [39]. However, the porous structures similar to Fig. 6 have also been reported [40].

Finally, the formation of silica on electrospun PEI/PVP fibers was confirmed by FTIR analysis of fibers before and after silicification and calcination (Fig. 7). Three important absorbance peaks that indicate the presence of silica include the following: –Si–OH stretching at 950 cm^{-1}, –Si–O–Si– symmetric stretching at 790 cm^{-1} and –Si–O– asymmetric stretching at 1090 cm^{-1} (each indicated by vertical reference lines in Fig. 7). Silica formation in the
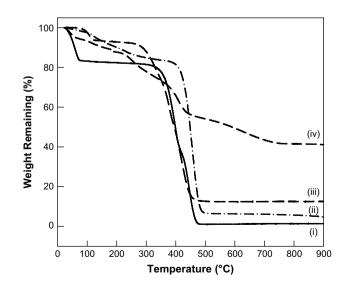

Fig. 5. TGA analysis of the silicified and non-silicified electrospun fibers of 50:50 blends of linear PEI and PVP (i) PEI:PVP fibers at ca. 40% humidity, (ii) silicified electrospun PVP fibers (control), (iii) silicified PEI:PVP fibers after exposure at ca. 40% humidity and (iv) silicified PEI:PVP fibers after exposure at ca. 80% humidity.
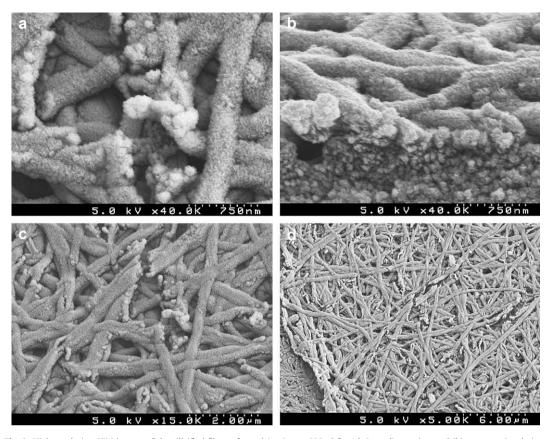
Fig. 6. High resolution SEM images of the silicified fibers after calcination at 600 °C for 1 h (a, c, d) top view and (b) cross-sectional view.

electrospun fibers is clearly evident from the –Si–O–Si– vibration band at 790 cm^{-1}, which is otherwise absent in the spectra of PEI/PVP fibers. Furthermore, a sharp peak at 1090 cm^{-1}, indicating a Si–O vibration appears in the silicified fibers. Interestingly, the Si–OH stretching mode at 950 cm^{-1} only has a slight increase in intensity compared to the siloxane (–Si–O–Si–) group at 790 cm^{-1}, implying quite complete condensation during silica polymerization. The increase in intensity of the broad peak around 3400 cm^{-1} assigned to –OH groups (indicated by * in Fig. 7), represents either the uncondensed silanol group or the –OH group in the water or alcohol liberated due to the condensation reactions of TMOS. The observed –OH peak occurred despite extensive drying of silicified fibers for 4 h at 40 °C in vacuum. Other peaks corresponding to various groups in PEI and PVP are also present in the region of 1200–2000 cm^{-1} and indicates very little or no change between non-silicified and silicified LPEI/PVP fibers. After calcination, all such organic peaks disappear, confirming the removal of organic content. The three main absorbance peaks corresponding to silica remain, as indicated by the vertical reference lines in the figures, thus further confirming the presence of silica. There remains a very weak peak at 950 cm^{-1} and 3400 cm^{-1} indicating a slight presence of uncondensed –Si–OH, in spite of calcination at 600 °C for 1 h. However, the later peak is very weak and is negligible compared to the other peaks in calcined fibers, indicating that most of the material in the calcined fibers is silica.

4. Discussion

The sol–gel synthesis of silica from such alkoxysilanes as TMOS proceeds via a two step reaction – (i) hydrolysis of the alkoxy (–Si–OCH$_3$) functional group to form silanol (Si–OH), and (ii)

condensation of such silanol group either with other alkoxy or silanol group to form the branched and networked siloxane (–Si–O–Si–) chains, liberating alcohol or water, respectively [18]. While the hydrolysis step occurs rapidly in presence of water and is usually catalyzed by acid or base, condensation is a slower and rate-limiting step, requiring between several hours to days for silica formation in absence of any flocculating agents or other external
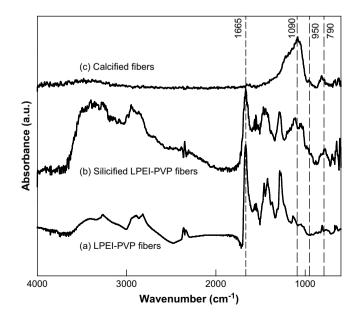

Fig. 7. FTIR of the electrospun PEI–PVP fibers (a) before silicification, (b) after silicification and (c) after calcination at 600 °C for 1 h.

catalyst. In contrast, the synthesis of silica as mediated by poly-amines that were isolated from silaffins is extremely rapid [41]. Similar to the catalytic ability of polyamines found in silaffins to form silica, we observed silica formation within minutes on electrospun PEI/PVP blends. The silica formed in the nanofibers cannot be merely due to the instantaneous hydrolysis and condensation of the TMOS. TMOS, while more active than tetraethylorthosilicate (TEOS) used in a conventional sol–gel process, was selected due to its ability to rapidly hydrolyze to silicic acid or its precursor molecules when in contact with water. However, subsequent condensation of the silicic acid is rate-limiting and it is believed that PEI helps to catalyze the formation of silica instantaneously on the fibers. This is in agreement with the previous solution study of silica formation from the linear PEI solution and gels [35,42,43]. In the absence of the PEI or other catalyst, the condensation step requires a long time (hours to days) to polymerize into silica. Adsorbed water in the nanofibers thus is required to hydrolyze TMOS and facilitate the first step of the chemical reaction toward silica formation. As such, the amount of water adsorbed on the fibers could be used to moderate and control the conversion of TMOS to silica nanofibers. Indeed, our results show that the silica content can be controlled by the water adsorbed into the fibers equilibrated at different humidities (Fig. 5). The SEM–EDX analysis (Fig. 3) and FTIR (Fig. 7) confirmed the presence of silica in the nanofibers. Such rapid silica formation in nanofibers occurs due to the unique catalytic ability of PEI to catalyze hydrolysis and/or condensation reactions of TMOS.

It is known that linear PEI crystallizes with double helix or a planar zig-zag structure if in the hydrated or dehydrated state, respectively [44]. DSC analysis (Fig. 4) of the electrospun nanofiber blend with PVP revealed that the PEI is crystalline in the nanofiber blends and further that e-spinning process enhanced the PEI crystallinity compared to the bulk PEI. Furthermore, the silica formation in the PEI nanofiber blend by TMOS exposure led to the disruption of the PEI crystals (Fig. 4). The silica formation by crystalline PEI observed in our study is in agreement with previous studies by Yuan and co-workers of silica formation in linear PEI solution and gels [33,36]. They reported that linear PEI can lead to gel formation in water by self-assembly of fibrous crystalline aggregates in aqueous solution (0.5–2 wt% PEI) [33] and that such aggregates were organized into a structure with crystalline core and a brush-like ethyleneimine segments [36]. Silicification of these crystalline PEI aggregates (in aqueous solution) was found to produce silica nanofibers (20–23 nm in diameter) with a core of axial, crystalline PEI filaments (5–7 nm in width) and a silica shell of 6–8 nm thick [36]. Interestingly, the length scale of silica reported in the previous studies is similar to the smallest length scale of the nanostructures (ca. 20 nm) observed in the SEM analysis of calcined nanofibers (Fig. 6). Indeed, our study confirms that silica formation can occur in the crystalline PEI nanofiber similar to the silica formation observed by the crystalline PEI aggregates in the solution.

Several mechanisms have been proposed for polyamine-assisted hydrolysis and condensation of the silica from precursor molecules. Sahai and Delak [45,46], studied the model compound trimethylethoxysilane (TMES) by ^{29}Si NMR at pH 5.0 and postulated a nucleophile-catalyzed mechanism of hydrolysis by polyamines. In particular, they concluded that the conjugated base of the amine attacks the silicon atom in organosilicate to form a penta-coordinated intermediate. They found that the hydrolysis rates are orders of magnitude higher than the condensation rates. Besides the hydrolysis reaction, researchers have found that PEI assists in the rapid condensation of the hydrolyzed precursor to form siloxane functional groups. According to the proposed mechanism for oligo-N-methyl-propylamine-assisted condensation [11,47], polyamine chains possess an alternation of protonated and non-protonated

amine groups along their backbone, with hydrogen bonds forming between two precursor acid (–Si–OH) groups and two adjacent repeating unit of the polyamine catalyst. Such complex formation facilitates Si–O bond formation by stabilizing the transition state. The hydrogen in each secondary amine group of the polyamines hydrogen bonds with the oxygen of forming silica, integrating the polyamines within the resulting composite material. Besides the hydrogen bond formation between amines in PEI and silica precursor, there also exists a possibility of hydrogen bond formation between with the carbonyl groups in PVP and amine group in PEI. This would lower the effectiveness of PEI in catalyzing silica formation. However, our DSC analysis (Fig. 4) indicates that the fibers are not a miscible blend of PEI and PVP, and hence there are large populations of both components (except at interface) not in molecular proximity for hydrogen bonding. Furthermore, PEI/PVP nanofibers blends were prepared as 50:50 blends by weight, leading to a 2.5:1 molar excess of hydrogen bond donors from PEI (44 g/mol-H) relative to hydrogen bond acceptors on PVP (111 g/mol-C=O). Thus, even if all of the carbonyls of PVP were saturated in hydrogen bonds from PEI, a significant concentration of secondary amines (ca. 3 of 5) would still be available to hydrogen bond with Si–OH to form silica in the presence of the precursor molecules.

In silaffins, where the catalytic domains consist of oligo-N-methyl-propylamine, the silica formed has a relative composition of 1.25:1 SiO_2/polyamine based on weight [41]; i.e., 55 wt% inorganic content. In our studies with PEI, the relative mass composition is expected to be 2:1 SiO_2/PEI, assuming that the silica formation from PEI occurs by the same mechanism mentioned above for N-methyl-propylamine, and considering the difference in repeat unit molar mass (43 g/mol for ethyleneimine versus 71 g/mol for N-methyl-propylamine). Accordingly, the silica/PEI composition should be ~66% inorganic. Further, in a 50/50 (w/w) blend of PEI/PVP, we expected around 33% inorganic content. Indeed, this simple argument agrees reasonably well with TGA results (Fig. 5) where the maximum inorganic content was 41% for the silicified PEI/PVP nanofibers exposed to 80% relative humidity prior to silicification. We speculate that the additional inorganic content observed (7%) might be due to secondary silica formation due to sol–gel synthesis, as described in more detail below.

The lower inorganic content of the PEI/PVP fibers exposed at lower than 80% relative humidity is clearly due to insufficient water to hydrolyze the TMOS for the silica formation. Thus, water plays an important role in the silica formation by PEI, as was also confirmed by negligible silica content of silicified fibers (Fig. 5) pre-treated at anhydrous conditions (<20% relative humidity). Our study signifies the importance of the water in the rapid silica formation within the fibers; however, quantification of the water content before silicification is needed to establish its effect, quantitatively, on silica content in fibers.

After the rapid silica formation by PEI in electrospun nanofibers, there exists a possibility of secondary silica formation due to condensation of alkoxysilanes or silanols with the surface silanol groups. However, we speculate that such an uncatalyzed process would be slow under ambient conditions and can be considered negligible for the 10 min allowed for immersion of the nanofibers in TMOS as was verified by TGA study for the fibers immersed for extended period of time. For the PEI/PVP fibers immersed in TMOS for 45 min, the inorganic content measured by TGA at 900 °C was 46.3 wt%, confirming the slow silica formation by the secondary sol–gel process (see Supplementary information, Figure S4). Such secondary silica formation may occur mainly on the fiber surface, increasing the fiber diameter. Eventually, the silica formed on the surface acts to weld the nanofibers to form a porous, solid-like structure at long immersion time (Supplementary information

Figure S5). However, in the case of the PEI/PVP fibers immersed in TMOS for only 1 min, the inorganic content by TGA was 31 wt%, which is slightly lower than the inorganic content of 41 wt% measured after 10 min TMOS immersion of nanofibers (Fig. 5), but close to that predicted for PEI catalysis (33 wt%) discussed above. Thus silica forms almost instantaneously in the nanofibers during the first few minutes of TMOS immersion, after which the non-catalyzed condensation of the TMOS or silicic acid proceeds at a lower rate.

5. Conclusions

Rapid formation of hybrid (polymer/silica) nanofibers was achieved by silicification of PEI/PVP electrospun nanofibers immersed in TMOS. PEI present in the nanofibers catalyzed near-instantaneous formation of silica – within minutes – resulting in a unique composite material. PVP fibers alone did not form silica when exposed to TMOS under similar conditions, confirming that the silica formation is induced by the PEI in the electrospun nanofibers of PEI/PVP blends. Silica formation was confirmed and characterized by FTIR, SEM–EDX, and TGA analyses. Compositionally, FTIR analysis indicated the presence of siloxane and silanol functional groups consistent with the formation of silica from TMOS while, morphologically, the fiber diameters showed a slight increase after silicification. DSC analysis revealed that PEI is crystalline in the nanofibers and that such crystallinity is disrupted by the silica formation in the nanofibers due to subsequent silicification by TMOS. Meanwhile, TGA analysis revealed that water is required for silica formation. In particular, relatively dry nanofibers did not afford silica formation, while fibers pre-treated at high relative humidity (80%) did. Furthermore, the highest inorganic content in the nanofibers was about 41% for the silicified fibers pre-treated at 80% relative humidity. Surprisingly, the inorganic content of the fibers immersed for just 1 min in TMOS yielded ~31% inorganic content. This finding was in agreement with the proposed mechanisms of the silica formation by polyamines where the formed silica closely interacts with the polyamines and results in 2:1 silica/polyamine by weight. Calcination of the silicified fiber mats led to porous ceramic nanofibers consisting of porous nano-structured silica fibrils. This biomimetic route to rapid synthesis of hybrid composite nanofibers could have widespread use, including diverse applications as catalysts, engineered tissued, and structural materials.

Supplementary information

(S1) SEM image of e-spun PEI fibers (S2) The diameter distribution of silicified and non-silicified PEI/PVP fibers for figure 1b and 2b and (S3) SEM image of the PVP fibers after 10 min TMOS immersion. (S4) TGA analysis of the silicified electrospun fibers for varying immersion time. (S5) SEM images of silicified electrospun fibers for varying immersion time. Supplementary data associated with this article can be found in the online version, at doi: 10.1016/j.polymer.2009.01.024.

References

[1] Lowenstam HA. Science (Washington, DC, United States) 1981;211(4487): 1126–31.
[2] Mann S. Angewandte Chemie, International Edition 2000;39(19):3392–406.
[3] Bauerlein E. Angewandte Chemie, International Edition 2003;42(6):614–41.
[4] Dujardin E, Mann S. Advanced Engineering Materials 2002;4(7):461–74.
[5] Estroff LA, Hamilton AD. Chemistry of Materials 2001;13(10):3227–35.
[6] Belcher AM, Hansma PK, Stucky GD, Morse DE. Acta Materialia 1998;46(3): 733–6.
[7] Mann S, Webb J, Williams RJP. Biomineralization: chemical and biochemical perspectives. Weinheim: VCH; 1989.
[8] Lowenstam HA, Weiner S. On biomineralization. New York: Oxford University Press; 1989.
[9] Kroger N, Deutzmann R, Sumper M. Science (Washington, D.C.) 1999; 286(5442):1129–32.
[10] Hildebrand M, Wetherbee R. Component sand control of silicification in diatoms. In: Muller WEG, editor. Silicon biomineralization: biology-biochemistry-molecular biology-biotechnology, vol. 33. Springer; 2003. p. 11–51.
[11] Pohnert G. Angewandte Chemie, International Edition 2002;41(17):3167–9.
[12] Patel AC, Li S, Wang C, Zhang W, Wei Y. Chemistry of Materials 2007;19(6): 1231–8.
[13] Patel AC, Li S, Yuan J-M, Wei Y. Nano Letters 2006;6(5):1042–6.
[14] Almeida RM, Goncalves MC, Portal S. Journal of Non-Crystalline Solids 2004;345–346:562–9.
[15] Kim H-W, Kim H-E, Knowles JC. Advanced Functional Materials 2006;16(12):1529–35.
[16] Zhang Y, Lim CT, Ramakrishna S, Huang Z-M. Journal of Materials Science: Materials in Medicine 2005;16(10):933–46.
[17] Sanchez C, Julian B, Belleville P, Popall M. Journal of Materials Chemistry 2005;15(35–36):3559–92.
[18] Iler RK. The chemistry of silica. New York: Wiley-Interscience; 1979.
[19] Douglas AL. Sol–gel processing of hybrid organic–inorganic materials based on polysilsesquioxanes. In: Prof. Dr. Guido K, editor. Hybrid materials; 2007. p. 225–54.
[20] Bellomo EG, Deming TJ. Journal of the American Chemical Society 2006;128(7):2276–9.
[21] Yuan YJ, Hentze HP, Arnold WM, Marlow BK, Antonietti M. Nano Letters 2002;2(12):1359–61.
[22] Jung JH, Ono Y, Sakurai K, Sano M, Shinkai S. Journal of the American Chemical Society 2000;122(36):8648–53.
[23] Caruso RA, Antonietti M. Chemistry of Materials 2001;13(10):3272–82.
[24] Li D, McCann JT, Xia Y, Marquez M. Journal of the American Ceramic Society 2006;89(6):1861–9.
[25] Chronakis IS. Journal of Materials Processing Technology 2005;167(2–3): 283–93.
[26] Choi S-S, Lee SG, Im SS, Kim SH, Joo YL. Journal of Materials Science Letters 2003;22(12):891–3.
[27] Larsen G, Velarde-Ortiz R, Minchow K, Barrero A, Loscertales IG. Journal of the American Chemical Society 2003;125(5):1154–5.
[28] Li D, Xia Y. Nano Letters 2004;4(5):933–8.
[29] Cha JN, Shimizu K, Zhou Y, Christiansen SC, Chmelka BF, Stucky GD, et al. Proceedings of the National Academy of Sciences of the United States of America 1999;96(2):361–5.
[30] Knecht Marc R, Wright David W. Chemical Communications (Cambridge, England) 2003;24:3038–9.
[31] Helmecke O, Hirsch A, Behrens P, Menzel H, Behrens P, Jahns M, et al. Handbook of biomineralization: biomimetic and bioinspired chemistry; 2007. p. 3–18.
[32] Patel PA, Polyelectrolyte multilayers: simulations, experiments, and applications in biomineralization. Macromolecular Science and Engineering, vol. Ph.D.: Case Western Reserve University; 2008. p. 279.
[33] Yuan J-J, Jin R-H. Advanced Materials (Weinheim, Germany) 2005;17(7): 885–8.
[34] Yuan J-J, Jin R-H. Langmuir 2005;21(7):3136–45.
[35]. Jin R-H, Yuan J-J. Macromolecular Chemistry and Physics 2005;206(21): 2160–70.
[36] Yuan J-J, Zhu P-X, Fukazawa N, Jin R-H. Advanced Functional Materials 2006;16(17):2205–12.
[37] Deitzel JM, Kleinmeyer J, Harris D, Beck Tan NC. Polymer 2000;42(1): 261–72.
[38] Jang SY, Seshadri V, Khil MS, Kumar A, Marquez M, Mather PT, et al. Advanced Materials 2005;17(18):2177–80.
[39] Brinker C, Scherer G. Sol–gel science: the physics and chemistry of sol–gel processing; 1990.
[40] Huang WL. Journal of Physics and Chemistry of Solids 2002;63(4):645.
[41] Kroger N, Deutzmann R, Bergsdorf C, Sumper M. Proceedings of the National Academy of Sciences of the United States of America 2000; 97(26):14133–8.
[42] Jin R-H, Yuan J-J. Journal of Materials Chemistry 2005;15(42):4513–7.
[43] Jin R-H, Yuan J-J. Chemical Communications (Cambridge, United Kingdom) 2005;11:1399–401.
[44] Chatani Y, Kobatake T, Tadokoro H. Macromolecules 1983;16(2):199–204.
[45] Delak Katya M, Sahai N. The Journal of Physical Chemistry. B, Condensed Matter, Materials, Surfaces, Interfaces & Biophysical 2006;110(36): 17819–29.
[46] Delak KM, Sahai N. Chemistry of Materials 2005;17(12):3221–7.
[47] Kroger N, Sumper M. In: Baeuerlein E, editor. Biomineralization. Weinheim: Wiley-VCH; 2000. p. 151–70.